NANOVLA: ROUTING DECOUPLED VISION-LANGUAGE UNDERSTANDING FOR NANO-SIZED GEN-ERALIST ROBOTIC POLICIES

Jiahong Chen* University of British Columbia Vancouver, Canada **Jing Wang*** University of Alberta Edmonton, Canada Long Chen Xiaomi EV Beijing, China

Chwei CaiNortheastern University
Vancouver, Canada

Jinghui Lu[†] Xiaomi EV Shanghai, China lujinghui@xiaomi.com

ABSTRACT

Vision-language-action (VLA) models have significantly advanced robotic manipulation by integrating vision-language models (VLMs), and action decoders into a unified architecture. However, their deployment on resource-constrained edge devices, such as mobile robots or embedded systems (e.g., Jetson Orin Nano), remains challenging due to high computational demands, especially in real-world scenarios where power, latency, and computational resources are critical. To close this gap, we introduce Nano-scale Vision-Language Action (NanoVLA), a family of lightweight VLA architectures that achieve high performance with minimal resources. Our core innovations include: (1) vision-language decoupling that moves conventional early vision and language inputs fusion in VLM to late stage, achieving better performance while enabling caching and reduce inference overhead and latency; (2) long-short action chunking to ensure smooth, coherent multistep planning without sacrificing real-time responsiveness; (3) dynamic routing that adaptively assigns lightweight or heavy backbones based on task complexity, further optimizing inference efficiency. Experimental results on several benchmarks, as well as real-world deployments, demonstrate that NanoVLA achieves up to 52x faster inference on edge devices compared to previous state-of-the-art VLA models, with 98% less parameters while maintaining or surpassing their task accuracy and generalization. Ablation studies confirm that our decoupling strategy preserves cross-task transferability, and the routing module enhances costperformance trade-offs, enabling practical, high-precision robotic manipulation on resource-constrained hardware.

1 Introduction

The conventional approach in robot learning has been to train task-specific models from scratch, but vision-language-action (VLA) models are emerging as a transformative paradigm (Brohan et al., 2022; Zitkovich et al., 2023; Mittal et al., 2023; Bjorck et al., 2025; Cheang et al., 2025). Built on pre-trained large language models (LLMs) (Yang et al., 2025a; Touvron et al., 2023; Team et al., 2024a; Cai et al., 2024) or vision-language models (VLMs) (Liu et al., 2023b; Chen et al., 2024; Beyer et al., 2024; Wang et al., 2024) with an appended action decoder, these models leverage webscale multi-modal pretraining to ground natural language instructions in diverse scenarios, enabling rapid adaptation across tasks with fine-tuning. This paradigm brings broad generalization to robot learning, but it clashes with the realities of deploying on resource-constrained edge hardware (e.g., Jetson Orin-class devices) for three key reasons: (1) inference remains slow and compute-intensive;

^{*}Equal contribution

[†]Corresponding author

(2) long-horizon behaviors often degrade into jerky or brittle motions; and (3) a single fixed backbone creates a mismatch between model capacity and task difficulty, resulting in overcomputing for simple actions and underperformance on long-horizon tasks. Consequently, the existing VLA models remain impractical outside datacenter-class machines (Wang et al., 2025).

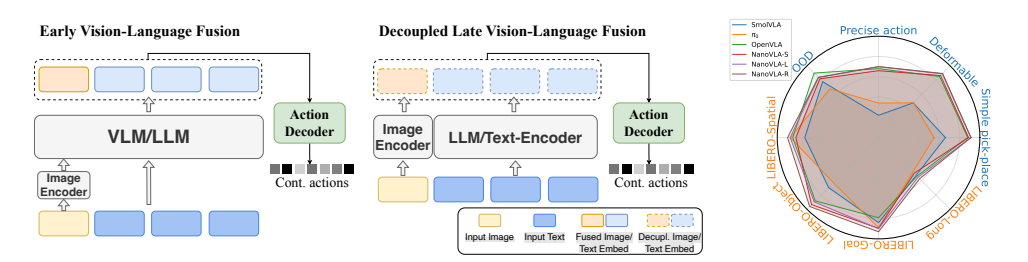


Figure 1: **Decoupled fusion for efficient VLA policies.** Our decoupled fusion strategy (mid) delays vision-to-language fusion in parameter-constrained settings. This approach does enables better performance with less overhead and latency, which informs NanoVLA, small scale VLA that achieves better performance across both simulation and real-world tasks with only $\sim 2\%$ of the parameter of models like OpenVLA, as shown in the Radar plot (right).

In response, we introduce **Nano**-scale **V**ision-Language **A**ction (NanoVLA), a framework that closes this deployment gap by reorganizing where modalities are fused, how actions are unrolled over time, and when a larger model backbone is invoked. As shown in Figure 1, rather than simply shrinking model parameters, NanoVLA reframes the inference around three complementary ideas that together deliver low latency and robust behavior on edge devices:

- Vision-language decoupling (cache what does not change). Most VLAs repeatedly interleave vision and language with heavy cross-attention, forcing the language backbone to recompute at every control step, even when the instruction remains the same. NanoVLA keeps vision and language separate until the last stage, so instruction features can be encoded once and reused, while only the image embedding and action module are updated per frame, resulting less computation. Notably, pre-trained visual and language encoders have learned highly abstract and semantically rich representations independently; delayed fusion helps avoid early cross-modal interference while preserving the individuality of each modality (Shukor et al., 2025b). Experimental results show that this design maintains competitive performance while improving efficiency.
- Long-short action chunking (plan long but act short). Step-by-step predictors are reactive but often jittery; long fixed chunks are smooth but unresponsive (Bharadhwaj et al., 2024; Zhao et al., 2023). NanoVLA strikes a balance: the policy generates a longer chunk of actions, but *executes only a short window* before re-planning with fresh observations. This amortizes expensive planning over multiple control steps, while keeping behavior smooth and adaptable to new visual evidence.
- **Dynamic Routing** (small backbone by default, large backbone on demand). NanoVLA incorporates a lightweight router that directs simple tasks (e.g., short-horizon grasps) to a compact language backbone, escalating to a larger backbone only when task difficulty increases. This adaptive approach maintains low average latency while preserving performance on complex tasks.

Taken together, these three components follow a single principle: *spend compute only where it matters*. **Decoupling** avoids redundant cross-modal computation; **chunking** ensures smooth long-horizon behavior with reactivity, and **routing** matches model capacity to task difficulty. With these strategies, NanoVLA turns a generalist policy into a practical edge controller, efficient in both architecture and inference, rather than merely a downsized replica of a large model. In summary, to the best of our knowledge, the proposed NanoVLA is the first VLA framework to integrate decoupled, cache-friendly vision-language processing, chunked long-horizon control, and adaptive backbone routing into a single edge-oriented design. We list our main contributions as follows:

We present a lightweight vision-language-action framework that makes large-model robot policies
practical on edge devices by rethinking where modalities are fused, how actions are executed over
time, and how compute is allocated.

- We demonstrate that our NanoVLA achieves a superior efficiency-effectiveness trade-off: it enables smooth long-horizon behaviors, low-latency inference, and adaptive capacity across varying task difficulties, capabilities not simultaneously supported by the existing VLAs.
- We validate NanoVLA on standard VLA benchmarks and real-world deployments, demonstrating
 that it matches or surpasses state-of-the-art performance while operating efficiently on resourceconstrained hardware.

2 Related Work

2.1 Large Language Models for Robotics

Large language models and their multi-modal extensions have recently become central to robot learning, which enables foundation robot policies that generalize across tasks, environments, and embodiments (Firoozi et al., 2025; Zhang et al., 2025b;a; Chen et al., 2025; Zhao et al., 2025; Zhou et al., 2025). By leveraging web-scale pretraining, such LLMs (Touvron et al., 2023; Beyer et al., 2024; Team et al., 2024a; Cai et al., 2024; Yang et al., 2025a) provide strong priors for semantic reasoning, while vision-language models (Liu et al., 2023b; Wang et al., 2024; Chen et al., 2024) leverage pre-trained visual encoder such as CLIP (Radford et al., 2021) and SigLIP (Zhai et al., 2023) to ground semantics in perception. This integration is most commonly realized in vision-language-action models, which pair visual encoders with LLM reasoning modules and action generators (e.g., action tokenizer (Kim et al., 2024), DDPM diffusion model (Kim et al., 2025) and flow matching model (Gao et al., 2024)).

2.2 Large-scale Generalist Policies

The availability of massive robot datasets, most notably Open-X-Embodiment (Collaboration et al., 2023), has enabled the development of large-scale generalist policies that rely heavily on scaling both architectures and data. OpenVLA (Kim et al., 2024) exemplifies this trend with a 7B-parameter VLM model trained on nearly one million trajectories, achieving state-of-the-art generalization across a wide variety of robotic tasks. π_0 (Black et al., 2024) and $\pi_{0.5}$ (Black et al., 2025) leverage self-supervised pretraining on web-scale multi-modal, demonstrating better zero-shot and open-world generalization, highlighting the effectiveness of scaling for learning broad semantics and grounding actions across tasks. However, such large scale models makes them impractical for the deployment on resource-constrained platforms, where low latency and compute efficiency are important. This mismatch has driven growing interest in compact alternatives that preserve generalization while improving efficiency (Shukor et al., 2025a; Wen et al., 2025; Yang et al., 2025b).

2.3 COMPACT AND EFFICIENT VLAS.

More recently, efforts have centered on designing smaller VLA models that maintain generalization while reducing the computational cost of deployment. RT-1 (Brohan et al., 2022) pioneered the generalist robotic models with only 35M parameters. Octo-Base (Team et al., 2024b) introduces a lightweight, 90M-parameter transformer policy trained on 800k trajectories, serving as an efficiency-oriented baseline. SmolVLA (Shukor et al., 2025a) takes this further by distilling knowledge from large VLAs into a compact 500M-parameter model, demonstrating that downsizing can preserve much of the generalization ability while reducing inference costs. These works signal a growing recognition that practical VLA deployment must address computational efficiency and edge hardware constraints, not only performance on datacenter GPUs.

3 NanoVLA

Deploying VLA models on edge devices requires more than shrinking parameters. It demands rethinking inference. The existing VLAs suffer from redundant cross-modal processing, brittle open-loop action execution, and fixed backbones that cannot adapt to task difficulty. To address these issues, NanoVLA introduces three design choices: (i) vision-language decoupling with caching, which avoids recomputing static instructions while updating visual inputs; (ii) long-short action chunking, which plans over long horizons but executes with frequent feedback; and (iii) dynamic

routing, which allocates computation adaptively by switching between lightweight and heavyweight backbones based on task complexity.

3.1 VISION-LANGUAGE DECOUPLING WITH CACHING

Modern VLA models demand heavy computation because they tightly interleave modalities through repeated cross-attention, forcing both vision and language backbones to recompute at every timestep. This design hinders real-time deployment on edge devices, where instructions often remain fixed while only the visual observations change. The existing work has shown that freezing large pretrained encoders and using lightweight adapters can preserve accuracy while reducing computation (Li et al., 2023). Building on this insight, our NanoVLA introduces a decoupled architecture that processes vision and language independently until a late fusion stage.

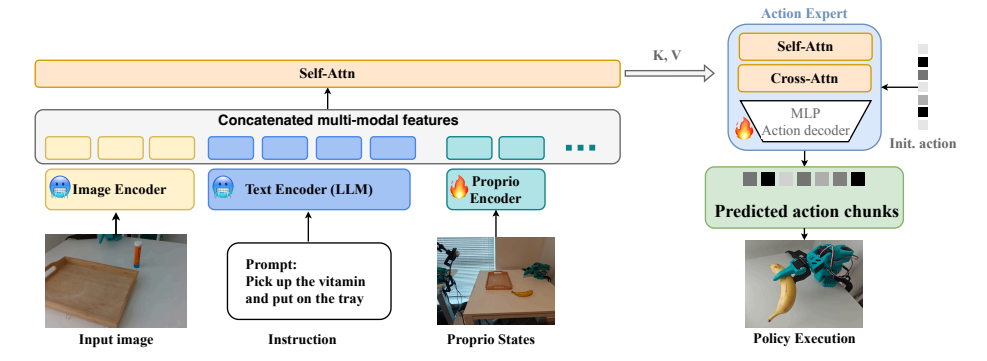


Figure 2: Overview of NanoVLA framework. Multi-modal inputs are processed independently and fused at a late stage via a lightweight attention layer. This design bypasses the compute-intensive early fusion in VLMs, unlocking key advantages like caching and accelerated inference.

Method. NanoVLA separates each input modality into its own encoder: a visual encoder (*e.g.*, ResNet (He et al., 2016), ViT (Dosovitskiy et al., 2020)) extracts compact scene features, while a language encoder (*e.g.*, BERT (Devlin et al., 2019), Qwen (Yang et al., 2025a)) encodes task instructions. Both encoders remain frozen during training, preserving their pretrained semantic knowledge and avoiding catastrophic forgetting. Additional modalities, such as proprioception, are incorporated via lightweight MLP projections and fused with self-attention. At the action-generation stage, we merge the modality-specific embeddings using a lightweight transformer. Each layer first applies self-attention over the output tokens, allowing the model to capture dependencies within the multi-modality features. Then, it applies cross-attention that fuses the visual and language features for action generation (see Appendix for details A.1). Because cross-modal attention is performed only once at this late stage, this design dramatically reduces redundant computation. This late fusion design bypasses the compute-intensive early cross-modal entanglement common in VLMs.

Caching for efficiency. A key advantage of this separation is the ability to cache intermediate features. For example, in an interactive robot setting, the instruction embedding needs to be computed only once and reused across timesteps, while the visual embedding is updated at every frame. This caching eliminates redundant computation and significantly reduces on-device latency, making inference practical on resource-constrained hardware.

The pretrained visual and language encoders produce rich and high-level semantic representations, as also observed in FrEVL (Bourigault & Bourigault, 2025), which the lightweight decoder can effectively fuse for accurate action prediction. By aligning computation with modality dynamics, which reuses stable instruction features while refreshing changing visual features, NanoVLA achieves competitive accuracy with far fewer trainable parameters and much faster inference.

3.2 Long-short Action Chunking

A second bottleneck for edge deployment arises from how actions are generated over time. Conventional chunking strategies (Zhao et al., 2023; Kim et al., 2025) predict a sequence of actions and then execute the entire chunk in an open-loop. While this reduces the number of forward passes, it

introduces a critical weakness: once a chunk is committed, the robot cannot correct for model mismatch, sensing latency, or environmental changes until the next replan. As a result, behaviors often become jerky, unstable, or misaligned in long-horizon tasks. Typically, real-world control requires two conflicting properties: *Temporal coherence*: Actions unfold smoothly across long horizons; *Responsiveness*: The policy can adapt quickly to new sensory input.

A fixed chunk size cannot satisfy both. If chunks are long, execution is smooth but brittle; if chunks are short, execution is reactive but jittery. Our goal is to retain the benefits of long-horizon planning while preserving frequent feedback during execution.

Method. In response, we propose **long-short action chunking (LSAC)**. During training, the policy is optimized to predict long sequences of actions, capturing temporal patterns and dependencies across horizons:

$$\mathbf{a}_{t:t+H_{\text{train}}-1} = \pi_{\theta}(x_t, l), \tag{1}$$

where x_t is the current observation, l is the task instruction, and H_{train} is the planning horizon. The training objective is supervised regression across the full chunk:

$$\mathcal{L}_{\text{chunk}}(\theta) = \frac{1}{H_{\text{train}}} \sum_{k=0}^{H_{\text{train}}-1} \ell(\pi_{\theta}(x_t, l)_k, a_{t+k}), \qquad (2)$$

where ℓ is an ℓ_1 or ℓ_2 loss. At inference time, however, the robot executes only the first $h \ll H_{\text{train}}$ actions of each predicted chunk before replanning with the latest observation:

$$\hat{\mathbf{a}}_{t:t+h-1} \leftarrow \pi_{\theta}(x_t, l)_{0:h}, \qquad t \leftarrow t + h, \text{ repeat.}$$
 (3)

This develops a long-short mismatch: the model plans over long horizons but acts in short bursts with frequent replanning. Overall, LSAC balances coherence and reactivity in long-horizon control. Training on long sequences promotes **smoothness**, executing short segments with replanning ensures **adaptability**, and predicting many steps per pass while acting on a few delivers **efficiency**. These properties together make LSAC well-suited for real-world robotic control on edge devices.

3.3 DYNAMIC ROUTING

A final challenge for efficient VLA deployment on edge devices is the mismatch between task difficulty and model capacity. A single fixed backbone wastes computation on simple instructions (e.g., short-horizon grasps) yet may still struggle with complex and reasoning-heavy tasks. What is needed is a mechanism to adaptively allocate compute, using lightweight models when possible and escalating to heavier ones only when necessary.

Method. Our NanoVLA introduces a **VLA router** that selects among candidate language models at inference time. Instead of relying on hard labels for routing (Ong et al., 2024), we estimate uncertainty-aware win probabilities between models. For each task $l \in \mathcal{T}$ and model $m \in \mathcal{M}$, we observe $n_{m,l}$ trials with $s_{m,l}$ successes, producing an empirical success rate $\hat{p}_{m,l} = \frac{s_{m,l}}{n_{m,l}}$. A router R chose a model for a new task l, trading off predicted performance and cost.

Bayesian success modeling. Rather than treating $\hat{p}_{m,l}$ as a point estimate, we place a Beta-Binomial model on the (unknown) per-task success probability to model uncertainty:

$$p_{m,l} \sim \text{Beta}(\alpha_{m,l}, \beta_{m,l}), \qquad \alpha_{m,l} = s_{m,l} + \alpha_0, \beta_{m,l} = (n_{m,l} - s_{m,l}) + \beta_0,$$
 (4)

with a weakly informative prior (we use $\alpha_0=\beta_0=1$ unless stated otherwise). This posterior reflects trial-count uncertainty: with few trials, posteriors are wider and induce probabilities closer to 1/2 in the pairwise comparisons below. Let $\mathcal D$ denote all observed trials.

Pairwise win probability. For any two models $i, j \in \mathcal{M}$ on task l, the win probability is defined:

$$\pi_{i \succ j}(l) = \Pr\left(p_{i,l} > p_{j,l} \middle| \mathcal{D}\right) = \int_0^1 \int_0^1 \mathbb{I}_{p_{i,l} > p_{j,l}} \operatorname{Beta}\left(p_{i,l}; \alpha_{i,l}, \beta_{i,l}\right) \operatorname{Beta}\left(p_{j,l}; \alpha_{j,l}, \beta_{j,l}\right) dp_{i,l} dp_{j,l}.$$
(5)

When $\alpha_{i,l} \in \mathbb{N}$, $\pi_{i \succ j}(l)$ admits the finite-sum closed form

$$\pi_{i \succ j}(l) = \sum_{k=0}^{\alpha_{i,l}-1} {\beta_{i,l} + k - 1 \choose k} \frac{B(\alpha_{j,l} + k, \beta_{i,l} + \beta_{j,l})}{B(\alpha_{j,l}, \beta_{j,l})}, \tag{6}$$

where $B(\cdot,\cdot)$ is the Beta function. To support non-integer hyperparameters uniformly, our **Monte Carlo-Beta** (MCB) estimator uses Monte Carlo: draw $x^{(r)} \sim \text{Beta}(\alpha_{i,l},\beta_{i,l})$ and $y^{(r)} \sim \text{Beta}(\alpha_{i,l},\beta_{i,l})$ for $r=1,\ldots,R$ and set

$$\widehat{\pi}_{i \succ j}(l) = \frac{1}{R} \sum_{r=1}^{R} \mathbb{I}_{x^{(r)} > y^{(r)}}.$$
(7)

We use the closed form equation 6 when applicable and otherwise fall back to the Monte Carlo estimator equation 7. Targets are clipped to $[\varepsilon, 1-\varepsilon]$ with $\varepsilon=10^{-4}$ for numerical stability.

Training objective. We train a text-conditioned binary classifier f_{θ} on serialized inputs (l, i, j) to predict $\Pr(i \succ j \mid l)$. Given the MCB target $\widehat{\pi}_{i \succ j}(l)$, we minimize the Bernoulli log-loss

$$\mathcal{L}\text{pair} = -\mathbb{E}_{l}, \mathbb{E}_{i < j} \left[\widehat{\pi}_{i \succ j}(l) \log \sigma(z_{i \succ j}(l)) + \left(1 - \widehat{\pi}_{i \succ j}(l)\right) \log \left(1 - \sigma(z_{i \succ j}(l))\right) \right], \tag{8}$$

where $z_{i\succ j}(l)$ is the model logit and σ is the logistic function. The win probabilities provide soft, calibrated supervision targets for training a text-conditioned binary classifier f_{θ} to predict $\Pr(i\succ j\mid l)$. At inference time, the router defaults to the lightweight model. It only escalates to the large model if the predicted success probability of the large model for task l, $\hat{p}_{L}(l)$, exceeds a threshold τ , which improves efficiency on simple tasks, and preserves accuracy on complex instructions.

4 EXPERIMENTS

To comprehensively evaluate our model's performance, we conducted experiments across a wide range of environmental setups, including 5 tasks in simulation environment and 12 tasks on real robots. We implemented three versions of NanoVLA, NanoVLA-S uses BERT-base as the text backbone, NanoVLA-L uses Qwen2.5 0.5B as the text backbone, and NanoVLA-R is the Router version. All models were using ResNet18 as the image encoder, and were trained with 100 AC steps with 10 AC steps during inference. We benchmark our approach against the following generalist policies: Octo-Base (Team et al., 2024b), OpenVLA (Kim et al., 2024), π_0 (Black et al., 2024), TraceVLA (Zheng et al., 2024), SpatialVLA (Qu et al., 2025), SmolVLA (Shukor et al., 2025a).

4.1 SIMULATED BENCHMARK

LIBERO is a standardized lifelong learning benchmark for VLA models (Liu et al., 2023a). In this experiment, we follow OpenVLA to use tasks from *LIBERO-Spatial*, *LIBERO-Object*, *LIBERO-Goal*, and the *LIBERO-Long*. These suites respectively emphasize spatial relations, object variation, goal (end-state) variation, and mixed/entangled tasks. We report the success rate (SR) of NanoVLA models as the average of 50 independent trails. For OpenVLA, TraceVLA, SpatialVLA, and Octo, we report the SR from their original paper. For π_0 and SmolVLA, we replicate the experiment from LeRobot code base with default setting (Cadene et al., 2024) and report the average SR, due to π_0 original paper did not provide the LIBERO results.

Benchmark	Policy	Total Params	Trainable Params	Spatial	Object	Goal	Long	Avg.
	Octo	90M	90M	78.9	85.7	84.6	51.1	75.1
	OpenVLA	7.5B	279M	84.7	88.4	79.2	53.7	76.5
	π_0	3.5B	3.1B	87.0	63.0	89.0	48.0	71.8
	TraceVLA	7B	7B	84.6	85.2	75.1	54.1	74.8
LIBERO	SpatialVLA	3.5B	50M	88.2	89.9	78.6	55.5	78.1
LIBERO	SmolVLA	450M	100M	72.8	69.8	84.0	52.6	78.6
	NanoVLA-S	161M	52M	81.6	93.6	89.6	49.8	78.7
	NanoVLA-L	520M	52M	87.2	89.8	90.0	55.2	80.4
	NanoVLA-R	296M*	52M	89.8	96.2	93.0	57.4	84.1

Table 1: Success rates (%) on four LIBERO task suites. Overall performance is calculated as the average over 50 test trials. (*total parameters calculated based on average L/S model invocation.)

Overall Performance. As shown in Table 1, NanoVLA consistently outperforms multi-Billion Parameter VLA models, such as OpenVLA, π_0 , TraceVLA, and SpatialVLA in the LIBERO tasks. NanoVLA shows significant performance gains, with improvements ranging from 6.0% to 12.3% in average success rates while only using less than 10% total parameters. When compared to other baselines like Octo-Base and SmolVLA, all NanoVLA models generally perform better, with fewer trainable parameters needed. These results suggest that the proposed NanoVLA framework can achieve generalized policy execution across various robotic manipulation tasks with significantly reduced model parameters, leading to improved performance-throughput trade-off in edge side executions. Especially, the proposed NanoVLA-R can further improve the precision by 3.7% while reducing 43% of the parameters of OpenVLA-L.

LIBERO-90. We further evaluate on *LIBERO-90* (90 short-horizon tasks), the official split of *LIBERO-100* designed to evaluate scalability and generalization across a broader and more diverse task distribution than the traditional four-suite setting. As shown in Table 2, our NanoVLA-L achieves the highest success (83.3%), with large absolute gains over compact and widely reported baselines (e.g., +14.4% over SmolVLA at 68.9% and +21.3% over OpenVLA at 62.0%), indicating stronger instruction following across many short-horizon skills rather than overfitting to a small set of controlled shifts. Notably, NanoVLA-S, which uses a weaker language backbone, performs worst among our variants (55.1%), suggesting the limitations of encoder-only language models in handling large-scale instruction following tasks. NanoVLA-R, also achieved 81.6% SR, which sacrificed 1.7% performance compared to NanoVLA-L while reducing the average total parameters by 41.0% to 307M.

Model	SmolVLA	OpenVLA	NanoVLA-S	NanoVLA-L	NanoVLA-R
LIBERO-90	68.9	62.0	55.1	83.3	81.6

Table 2: Results on LIBERO-90 benchmark (%).

4.2 REAL-WORLD VALIDATION

We evaluate NanoVLA on the easy to access and low cost LeRobot and edge-side device Jetson Orin Nano (8GB). Below we introduce the experiment set up for the robots and the results.

LeRobot. As shown in Figure 3, we assembled LeRobot So-arm 101 for robot manipulation tasks using a fixed-mounted third-person view camera capturing default 1280×720 RGB images. We collected 50 demonstration trajectories per task and merged them together for finetuning. The detailed real-world experimental setup and protocols are presented in Appendix A.2.



Figure 3: **LeRobot experiment setup**. We design 10 real-world tasks with different manipulation skills and objects with additional 2 unseen tasks for evaluating policy generalization.

As shown in Table 3, NanoVLA consistently outperforms the baseline across diverse tasks including pick-and-place operations, precise object movement, and deformable object manipulation. Notably, in easier pick-place tasks, NanoVLA-S (161M parameters) can even outperform OpenVLA (7B parameters), which has 43.5x more parameters. For deformable object such as banana and towel, all NanoVLA-based models achieved 90%+ success rate, beating all basesline. Additionally, for more complex tasks such open/close lid that require precise action generation, Nano-VLA can also consistently outperform baselines. Furthermore, we evaluate the NanoVLA's generalization capabilities, we conducted additional experiments with two out-of-domain (OOD) tasks for both unseen tasks and unseen objects. The results in Table 3 demonstrates NanoVLA generalization capability on unseen tasks due to its superior capability in language grounding.

	Task	SmolVLA	π_0	OpenVLA	Nano-S	Nano-L	Nano-R
Simple pick-place	Pick-place vitamin	64.0	36.0	90.0	96.0	96.0	96.0
	Pick-place spoon	58.0	46.0	88.0	92.0	90.0	92.0
	Pick-place USB drive	80.0	64.0	74.0	76.0	82.0	80.0
	Pick-place toothpaste	84.0	76.0	94.0	88.0	92.0	92.0
	Pick-place juice box	44.0	52.0	94.0	92.0	96.0	96.0
Precise Deformable	Pick-place banana	32.0	40.0	86.0	94.0	90.0	92.0
	Pick-place tissue	78.0	62.0	90.0	92.0	98.0	98.0
	Move towel right	22.0	34.0	68.0	66.0	70.0	70.0
Precise	Open lid	54.0	48.0	56.0	54.0	76.0	72.0
	Close lid	44.0	42.0	54.0	42.0	68.0	70.0
poo	OOD pick-place	78.0	68.0	90.0	82.0	84.0	84.0
	Avg.	58.0	51.6	80.4	79.5	85.6	85.6

Table 3: Performance comparison of NanoVLA (i.e., Nano-S, Nano-L and Nano-R) models and baselines on 11 real-world LeRobot manipulation tasks.

4.3 Inference Latency Analysis

To validate the effectiveness of the edge-side deployment for NanoVLA family, we deployed them on the *Jetson Orin Nano Super Developer Kit*, which has 8GB memory with CUDA support and a computation performance for up to 67 TOPS. For fair comparison, we report the results in following sections on publicly available LIBERO-Goal. As shown in Figure 4a, NanoVLA outperforms OpenVLA¹, achieving 52x higher FPS and +13.8% SR. When comparing the smaller SmolVLA, NanoVLA with 10 action-chunk (AC) steps is only slightly slower (-17.1%) than SmolVLA at 50 AC steps; when matching 50 AC steps, NanoVLA shows a minor SR decrease from ~90% to 87.2%, which is still 3.2% above SmolVLA, while delivering 43.8% higher FPS. We also evaluate the training efficiency of NanoVLA, as detailed in Appendix A.5.

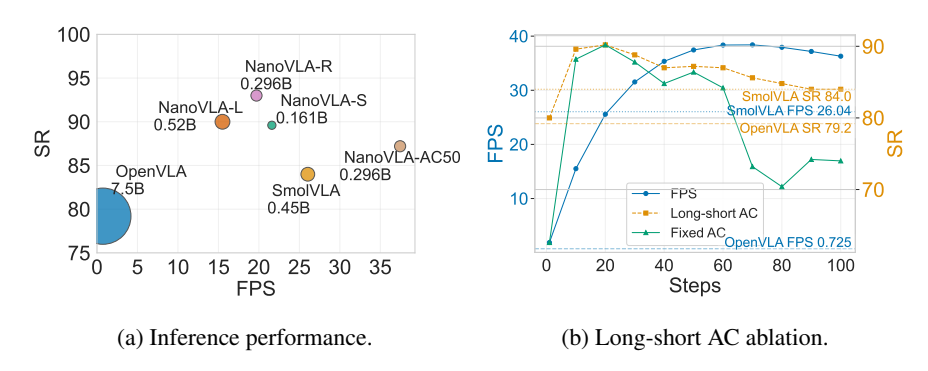


Figure 4: Inference analysis on Jetson Orin Nano (left) and long-short action chunking ablations.

4.4 ABLATION STUDIES

Long-short action chunking effectiveness. We also compare success rate for traditional fixed action-chunking (AC) and our long-short AC while also reporting throughput (FPS) across step sizes. As shown in Figure 4b, both methods peak at 20 steps (90.2 SR), but their behaviors diverge thereafter. Long-short AC maintains a high, flat SR plateau from 20-60 steps, then decays gently to 84.0 by 100 steps. Fixed AC is unstable beyond 30-40 steps, dropping sharply after 60 to 70-74 SR. Additionally, throughput increases with step size for both methods, which yields favorable operating points where long-short AC simultaneously surpasses the SmolVLA reference. Overall, long-short AC offers a superior SR-throughput trade-off and markedly better stability across step sizes. It's

¹Note that even 4-bit OpenVLA will result in out-of-memory, we report the frames per second (FPS) of OpenVLA using the data from the 4-bit Llama2 model, which is the text backbone of OpenVLA

also more flexible in real-world deployment as it only need to train once. It preserves near-peak SR over a wide range while allowing the system to dial up steps to increase FPS with only modest SR loss, whereas fixed AC suffers a steep accuracy collapse at larger steps.

Environmental Variant Impact. Figure 5a demonstrates environmental conditions' impact on policy execution. We collected the real-world training data during night time, and conducted the test in both day and night time. Apart from lighting condition changes, robot arm and goal object's shadow will impact the image understanding. Notably, NanoVLA shows substantial enhancements over baselines, with an SR improvement between 8.5% to 42.1% in average performance. The use of continuous action decoder while freezing decoupled LLM and image encoder proves particularly effective when encountering the environmental shift, as the LLM generated action embeddings won't be significantly impacted by the image embeddings, which can provide robust trajectory generation. This helps the model maintain policy execution SR despite changes in environments.

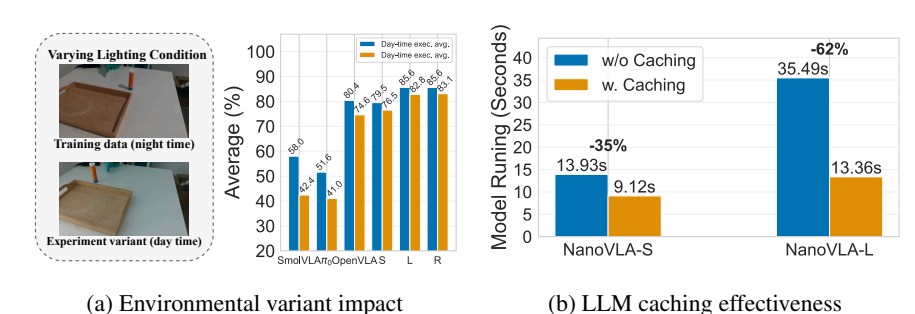


Figure 5: Ablation studies on environmental variant impact (left) and caching effectiveness (right).

LLM caching throughput. As shown in Figure 5b, when using Qwen 0.5B as the backbone, caching mechanism can save 62% inference time per execution task due to the LLM decoupling mechanism in the NanoVLA. Additionally, for smaller backbone such as BERT-base, we also observed a 35% inference time reduction, suggesting the efficiency of the decoupling method.

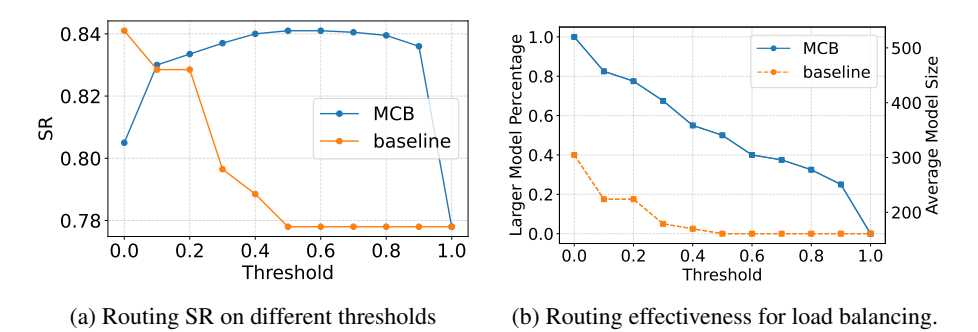


Figure 6: MCB Routing Effectiveness

Routing efficiency. We analyze the effect of the decision threshold on SR-compute trade-offs for the proposed MCB router. Figure 6a presents Routing SR on LIBERO task suites under different thresholds. As a result of routing, the SR increases from 0.805 (NanoVLA-L only) at τ =0 to a broad plateau around 0.84 spanning $\tau \in [0.4, 0.9]$ (mixture of NanoVLA-S/L. Additionally, as presented in Figure 6b, the routing module successfully reduces the average model size from NanoVLA-L's 520M to 251M while increasing the performance from 80.5% to 83.6%. it also significant increases NanoVLA-S's performance by 5.8% from 77.8% to 83.6%, while only increases the average number of parameters from 161M to 251M. This presents effectiveness of the proposed MCB router in selecting most effective model in various tasks. When comparing to the naive baseline which selects the model purely based on SR, the proposed MCB approach present a wider operating range, while the baseline is highly sensitive to threshold choice. MCB is robust to mis-calibration and task heterogeneity obtain near-maximal precision based on the computational resources, whereas the baseline requires staying very close to $\tau=0$ to avoid a substantial accuracy penalty.

5 Conclusion

We presented NanoVLA, a lightweight VLA framework that makes foundational robot policies practical on edge devices. Through decoupling with caching, long-short chunking, and dynamic routing, it delivers smooth long-horizon behaviors, low-latency inference, and adaptive compute allocation. Experiments on benchmarks and real robots demonstrate that NanoVLA matches or surpasses state-of-the-art VLAs while running efficiently on resource-constrained hardware, offering a practical path toward scalable real-time embodied AI.

REFERENCES

- Lucas Beyer, Andreas Steiner, André Susano Pinto, Alexander Kolesnikov, Xiao Wang, Daniel Salz, Maxim Neumann, Ibrahim Alabdulmohsin, Michael Tschannen, Emanuele Bugliarello, et al. Paligemma: A versatile 3b vlm for transfer. *arXiv preprint arXiv:2407.07726*, 2024.
- Homanga Bharadhwaj, Jay Vakil, Mohit Sharma, Abhinav Gupta, Shubham Tulsiani, and Vikash Kumar. Roboagent: Generalization and efficiency in robot manipulation via semantic augmentations and action chunking. In 2024 IEEE International Conference on Robotics and Automation (ICRA), pp. 4788–4795. IEEE, 2024.
- Johan Bjorck, Fernando Castañeda, Nikita Cherniadev, Xingye Da, Runyu Ding, Linxi Fan, Yu Fang, Dieter Fox, Fengyuan Hu, Spencer Huang, et al. Gr00t n1: An open foundation model for generalist humanoid robots. *arXiv preprint arXiv:2503.14734*, 2025.
- Kevin Black, Noah Brown, Danny Driess, Adnan Esmail, Michael Equi, Chelsea Finn, Niccolo Fusai, Lachy Groom, Karol Hausman, Brian Ichter, et al. *pi*₋0: A vision-language-action flow model for general robot control. *arXiv preprint arXiv:2410.24164*, 2024.
- Kevin Black, Noah Brown, James Darpinian, Karan Dhabalia, Danny Driess, Adnan Esmail, Michael Equi, Chelsea Finn, Niccolo Fusai, Manuel Y Galliker, et al. $\pi 0.5$: a vision-language-action model with open-world generalization. *arXiv preprint arXiv:2504.16054*, 2025.
- Emmanuelle Bourigault and Pauline Bourigault. Frevl: Leveraging frozen pretrained embeddings for efficient vision-language understanding. *arXiv preprint arXiv:2508.04469*, 2025.
- Anthony Brohan, Noah Brown, Justice Carbajal, Yevgen Chebotar, Joseph Dabis, Chelsea Finn, Keerthana Gopalakrishnan, Karol Hausman, Alex Herzog, Jasmine Hsu, et al. Rt-1: Robotics transformer for real-world control at scale. *arXiv preprint arXiv:2212.06817*, 2022.
- Remi Cadene, Simon Alibert, Alexander Soare, Quentin Gallouedec, Adil Zouitine, Steven Palma, Pepijn Kooijmans, Michel Aractingi, Mustafa Shukor, Dana Aubakirova, Martino Russi, Francesco Capuano, Caroline Pascal, Jade Choghari, Jess Moss, and Thomas Wolf. Lerobot: State-of-the-art machine learning for real-world robotics in pytorch. https://github.com/huggingface/lerobot, 2024.
- Zheng Cai, Maosong Cao, Haojiong Chen, Kai Chen, Keyu Chen, Xin Chen, Xun Chen, Zehui Chen, Zhi Chen, Pei Chu, et al. Internlm2 technical report. *arXiv preprint arXiv:2403.17297*, 2024.
- Chilam Cheang, Sijin Chen, Zhongren Cui, Yingdong Hu, Liqun Huang, Tao Kong, Hang Li, Yifeng Li, Yuxiao Liu, Xiao Ma, et al. Gr-3 technical report. *arXiv preprint arXiv:2507.15493*, 2025.
- Kaiyuan Chen, Shuangyu Xie, Zehan Ma, Pannag R Sanketi, and Ken Goldberg. Robo2vlm: Visual question answering from large-scale in-the-wild robot manipulation datasets. arXiv preprint arXiv:2505.15517, 2025.
- Zhe Chen, Jiannan Wu, Wenhai Wang, Weijie Su, Guo Chen, Sen Xing, Muyan Zhong, Qinglong Zhang, Xizhou Zhu, Lewei Lu, et al. Internvl: Scaling up vision foundation models and aligning for generic visual-linguistic tasks. In *Proceedings of the IEEE/CVF conference on computer vision and pattern recognition*, pp. 24185–24198, 2024.

Open X-Embodiment Collaboration, Abby O'Neill, Abdul Rehman, Abhinav Gupta, Abhiram Maddukuri, Abhishek Gupta, Abhishek Padalkar, Abraham Lee, Acorn Pooley, Agrim Gupta, Ajay Mandlekar, Ajinkya Jain, Albert Tung, Alex Bewley, Alex Herzog, Alex Irpan, Alexander Khazatsky, Anant Rai, Anchit Gupta, Andrew Wang, Andrey Kolobov, Anikait Singh, Animesh Garg, Aniruddha Kembhavi, Annie Xie, Anthony Brohan, Antonin Raffin, Archit Sharma, Arefeh Yavary, Arhan Jain, Ashwin Balakrishna, Ayzaan Wahid, Ben Burgess-Limerick, Beomjoon Kim, Bernhard Schölkopf, Blake Wulfe, Brian Ichter, Cewu Lu, Charles Xu, Charlotte Le, Chelsea Finn, Chen Wang, Chenfeng Xu, Cheng Chi, Chenguang Huang, Christine Chan, Christopher Agia, Chuer Pan, Chuyuan Fu, Coline Devin, Danfei Xu, Daniel Morton, Danny Driess, Daphne Chen, Deepak Pathak, Dhruv Shah, Dieter Büchler, Dinesh Jayaraman, Dmitry Kalashnikov, Dorsa Sadigh, Edward Johns, Ethan Foster, Fangchen Liu, Federico Ceola, Fei Xia, Feiyu Zhao, Felipe Vieira Frujeri, Freek Stulp, Gaoyue Zhou, Gaurav S. Sukhatme, Gautam Salhotra, Ge Yan, Gilbert Feng, Giulio Schiavi, Glen Berseth, Gregory Kahn, Guangwen Yang, Guanzhi Wang, Hao Su, Hao-Shu Fang, Haochen Shi, Henghui Bao, Heni Ben Amor, Henrik I Christensen, Hiroki Furuta, Homanga Bharadhwaj, Homer Walke, Hongjie Fang, Huy Ha, Igor Mordatch, Ilija Radosavovic, Isabel Leal, Jacky Liang, Jad Abou-Chakra, Jaehyung Kim, Jaimyn Drake, Jan Peters, Jan Schneider, Jasmine Hsu, Jay Vakil, Jeannette Bohg, Jeffrey Bingham, Jeffrey Wu, Jensen Gao, Jiaheng Hu, Jiajun Wu, Jialin Wu, Jiankai Sun, Jianlan Luo, Jiayuan Gu, Jie Tan, Jihoon Oh, Jimmy Wu, Jingpei Lu, Jingyun Yang, Jitendra Malik, João Silvério, Joey Hejna, Jonathan Booher, Jonathan Tompson, Jonathan Yang, Jordi Salvador, Joseph J. Lim, Junhyek Han, Kaiyuan Wang, Kanishka Rao, Karl Pertsch, Karol Hausman, Keegan Go, Keerthana Gopalakrishnan, Ken Goldberg, Kendra Byrne, Kenneth Oslund, Kento Kawaharazuka, Kevin Black, Kevin Lin, Kevin Zhang, Kiana Ehsani, Kiran Lekkala, Kirsty Ellis, Krishan Rana, Krishnan Srinivasan, Kuan Fang, Kunal Pratap Singh, Kuo-Hao Zeng, Kyle Hatch, Kyle Hsu, Laurent Itti, Lawrence Yunliang Chen, Lerrel Pinto, Li Fei-Fei, Liam Tan, Linxi "Jim" Fan, Lionel Ott, Lisa Lee, Luca Weihs, Magnum Chen, Marion Lepert, Marius Memmel, Masayoshi Tomizuka, Masha Itkina, Mateo Guaman Castro, Max Spero, Maximilian Du, Michael Ahn, Michael C. Yip, Mingtong Zhang, Mingyu Ding, Minho Heo, Mohan Kumar Srirama, Mohit Sharma, Moo Jin Kim, Muhammad Zubair Irshad, Naoaki Kanazawa, Nicklas Hansen, Nicolas Heess, Nikhil J Joshi, Niko Suenderhauf, Ning Liu, Norman Di Palo, Nur Muhammad Mahi Shafiullah, Oier Mees, Oliver Kroemer, Osbert Bastani, Pannag R Sanketi, Patrick "Tree" Miller, Patrick Yin, Paul Wohlhart, Peng Xu, Peter David Fagan, Peter Mitrano, Pierre Sermanet, Pieter Abbeel, Priya Sundaresan, Qiuyu Chen, Quan Vuong, Rafael Rafailov, Ran Tian, Ria Doshi, Roberto Mart'in-Mart'in, Rohan Baijal, Rosario Scalise, Rose Hendrix, Roy Lin, Runjia Qian, Ruohan Zhang, Russell Mendonca, Rutav Shah, Ryan Hoque, Ryan Julian, Samuel Bustamante, Sean Kirmani, Sergey Levine, Shan Lin, Sherry Moore, Shikhar Bahl, Shivin Dass, Shubham Sonawani, Shubham Tulsiani, Shuran Song, Sichun Xu, Siddhant Haldar, Siddharth Karamcheti, Simeon Adebola, Simon Guist, Soroush Nasiriany, Stefan Schaal, Stefan Welker, Stephen Tian, Subramanian Ramamoorthy, Sudeep Dasari, Suneel Belkhale, Sungjae Park, Suraj Nair, Suvir Mirchandani, Takayuki Osa, Tanmay Gupta, Tatsuya Harada, Tatsuya Matsushima, Ted Xiao, Thomas Kollar, Tianhe Yu, Tianli Ding, Todor Davchev, Tony Z. Zhao, Travis Armstrong, Trevor Darrell, Trinity Chung, Vidhi Jain, Vikash Kumar, Vincent Vanhoucke, Vitor Guizilini, Wei Zhan, Wenxuan Zhou, Wolfram Burgard, Xi Chen, Xiangyu Chen, Xiaolong Wang, Xinghao Zhu, Xinyang Geng, Xiyuan Liu, Xu Liangwei, Xuanlin Li, Yansong Pang, Yao Lu, Yecheng Jason Ma, Yejin Kim, Yevgen Chebotar, Yifan Zhou, Yifeng Zhu, Yilin Wu, Ying Xu, Yixuan Wang, Yonatan Bisk, Yongqiang Dou, Yoonyoung Cho, Youngwoon Lee, Yuchen Cui, Yue Cao, Yueh-Hua Wu, Yujin Tang, Yuke Zhu, Yunchu Zhang, Yunfan Jiang, Yunshuang Li, Yunzhu Li, Yusuke Iwasawa, Yutaka Matsuo, Zehan Ma, Zhuo Xu, Zichen Jeff Cui, Zichen Zhang, Zipeng Fu, and Zipeng Lin. Open X-Embodiment: Robotic learning datasets and RT-X models. https://arxiv.org/abs/2310.08864,2023.

Jacob Devlin, Ming-Wei Chang, Kenton Lee, and Kristina Toutanova. Bert: Pre-training of deep bidirectional transformers for language understanding. In *Proceedings of the 2019 conference of the North American chapter of the association for computational linguistics: human language technologies, volume 1 (long and short papers)*, pp. 4171–4186, 2019.

Alexey Dosovitskiy, Lucas Beyer, Alexander Kolesnikov, Dirk Weissenborn, Xiaohua Zhai, Thomas Unterthiner, Mostafa Dehghani, Matthias Minderer, Georg Heigold, Sylvain Gelly, et al. An image is worth 16x16 words: Transformers for image recognition at scale. *arXiv* preprint *arXiv*:2010.11929, 2020.

- Roya Firoozi, Johnathan Tucker, Stephen Tian, Anirudha Majumdar, Jiankai Sun, Weiyu Liu, Yuke Zhu, Shuran Song, Ashish Kapoor, Karol Hausman, et al. Foundation models in robotics: Applications, challenges, and the future. *The International Journal of Robotics Research (IJRR)*, 44 (5):701–739, 2025.
- Chongkai Gao, Haozhuo Zhang, Zhixuan Xu, Zhehao Cai, and Lin Shao. Flip: Flow-centric generative planning as general-purpose manipulation world model. arXiv preprint arXiv:2412.08261, 2024.
- Kaiming He, Xiangyu Zhang, Shaoqing Ren, and Jian Sun. Deep residual learning for image recognition. In *Proceedings of the IEEE conference on computer vision and pattern recognition*, pp. 770–778, 2016.
- Moo Jin Kim, Karl Pertsch, Siddharth Karamcheti, Ted Xiao, Ashwin Balakrishna, Suraj Nair, Rafael Rafailov, Ethan Foster, Grace Lam, Pannag Sanketi, et al. Openvla: An open-source vision-language-action model. *arXiv preprint arXiv:2406.09246*, 2024.
- Moo Jin Kim, Chelsea Finn, and Percy Liang. Fine-tuning vision-language-action models: Optimizing speed and success. *arXiv preprint arXiv:2502.19645*, 2025.
- Junnan Li, Dongxu Li, Silvio Savarese, and Steven Hoi. Blip-2: Bootstrapping language-image pre-training with frozen image encoders and large language models. In *International conference on machine learning*, pp. 19730–19742. PMLR, 2023.
- Bo Liu, Yifeng Zhu, Chongkai Gao, Yihao Feng, Qiang Liu, Yuke Zhu, and Peter Stone. Libero: Benchmarking knowledge transfer for lifelong robot learning. *Advances in Neural Information Processing Systems*, 36:44776–44791, 2023a.
- Haotian Liu, Chunyuan Li, Qingyang Wu, and Yong Jae Lee. Visual instruction tuning. *Advances in neural information processing systems*, 36:34892–34916, 2023b.
- Mayank Mittal, Calvin Yu, Qinxi Yu, Jingzhou Liu, Nikita Rudin, David Hoeller, Jia Lin Yuan, Ritvik Singh, Yunrong Guo, Hammad Mazhar, Ajay Mandlekar, Buck Babich, Gavriel State, Marco Hutter, and Animesh Garg. Orbit: A unified simulation framework for interactive robot learning environments. *IEEE Robotics and Automation Letters*, 8(6):3740–3747, 2023. doi: 10.1109/LRA.2023.3270034.
- Isaac Ong, Amjad Almahairi, Vincent Wu, Wei-Lin Chiang, Tianhao Wu, Joseph E Gonzalez, M Waleed Kadous, and Ion Stoica. Routellm: Learning to route llms with preference data. *arXiv* preprint arXiv:2406.18665, 2024.
- Delin Qu, Haoming Song, Qizhi Chen, Yuanqi Yao, Xinyi Ye, Yan Ding, Zhigang Wang, JiaYuan Gu, Bin Zhao, Dong Wang, et al. Spatialvla: Exploring spatial representations for visual-language-action model. *arXiv preprint arXiv:2501.15830*, 2025.
- Alec Radford, Jong Wook Kim, Chris Hallacy, Aditya Ramesh, Gabriel Goh, Sandhini Agarwal, Girish Sastry, Amanda Askell, Pamela Mishkin, Jack Clark, et al. Learning transferable visual models from natural language supervision. In *International Conference on Machine Learning (ICML)*, pp. 8748–8763. PmLR, 2021.
- Mustafa Shukor, Dana Aubakirova, Francesco Capuano, Pepijn Kooijmans, Steven Palma, Adil Zouitine, Michel Aractingi, Caroline Pascal, Martino Russi, Andres Marafioti, et al. Smolvla: A vision-language-action model for affordable and efficient robotics. *arXiv preprint arXiv:2506.01844*, 2025a.
- Mustafa Shukor, Enrico Fini, Victor Guilherme Turrisi da Costa, Matthieu Cord, Joshua Susskind, and Alaaeldin El-Nouby. Scaling laws for native multimodal models. *arXiv preprint arXiv:2504.07951*, 2025b.
- Gemma Team, Thomas Mesnard, Cassidy Hardin, Robert Dadashi, Surya Bhupatiraju, Shreya Pathak, Laurent Sifre, Morgane Rivière, Mihir Sanjay Kale, Juliette Love, et al. Gemma: Open models based on gemini research and technology. *arXiv preprint arXiv:2403.08295*, 2024a.

- Octo Model Team, Dibya Ghosh, Homer Walke, Karl Pertsch, Kevin Black, Oier Mees, Sudeep Dasari, Joey Hejna, Tobias Kreiman, Charles Xu, et al. Octo: An open-source generalist robot policy. *arXiv preprint arXiv:2405.12213*, 2024b.
- Hugo Touvron, Louis Martin, Kevin Stone, Peter Albert, Amjad Almahairi, Yasmine Babaei, Nikolay Bashlykov, Soumya Batra, Prajjwal Bhargava, Shruti Bhosale, et al. Llama 2: Open foundation and fine-tuned chat models. *arXiv preprint arXiv:2307.09288*, 2023.
- Hongyu Wang, Chuyan Xiong, Ruiping Wang, and Xilin Chen. Bitvla: 1-bit vision-language-action models for robotics manipulation. *arXiv* preprint arXiv:2506.07530, 2025.
- Peng Wang, Shuai Bai, Sinan Tan, Shijie Wang, Zhihao Fan, Jinze Bai, Keqin Chen, Xuejing Liu, Jialin Wang, Wenbin Ge, et al. Qwen2-vl: Enhancing vision-language model's perception of the world at any resolution. *arXiv* preprint arXiv:2409.12191, 2024.
- Junjie Wen, Yichen Zhu, Jinming Li, Minjie Zhu, Zhibin Tang, Kun Wu, Zhiyuan Xu, Ning Liu, Ran Cheng, Chaomin Shen, et al. Tinyvla: Towards fast, data-efficient vision-language-action models for robotic manipulation. *IEEE Robotics and Automation Letters*, 2025.
- An Yang, Anfeng Li, Baosong Yang, Beichen Zhang, Binyuan Hui, Bo Zheng, Bowen Yu, Chang Gao, Chengen Huang, Chenxu Lv, et al. Qwen3 technical report. *arXiv preprint arXiv:2505.09388*, 2025a.
- Yantai Yang, Yuhao Wang, Zichen Wen, Luo Zhongwei, Chang Zou, Zhipeng Zhang, Chuan Wen, and Linfeng Zhang. Efficientvla: Training-free acceleration and compression for vision-language-action models. *arXiv preprint arXiv:2506.10100*, 2025b.
- Xiaohua Zhai, Basil Mustafa, Alexander Kolesnikov, and Lucas Beyer. Sigmoid loss for language image pre-training. In *Proceedings of the IEEE/CVF International Conference on Computer Vision (ICCV)*, pp. 11975–11986, 2023.
- Wenbo Zhang, Tianrun Hu, Yanyuan Qiao, Hanbo Zhang, Yuchu Qin, Yang Li, Jiajun Liu, Tao Kong, Lingqiao Liu, and Xiao Ma. Chain-of-action: Trajectory autoregressive modeling for robotic manipulation. *arXiv preprint arXiv:2506.09990*, 2025a.
- Wenyao Zhang, Hongsi Liu, Zekun Qi, Yunnan Wang, Xinqiang Yu, Jiazhao Zhang, Runpei Dong, Jiawei He, He Wang, Zhizheng Zhang, et al. Dreamvla: a vision-language-action model dreamed with comprehensive world knowledge. *arXiv preprint arXiv:2507.04447*, 2025b.
- Tony Z Zhao, Vikash Kumar, Sergey Levine, and Chelsea Finn. Learning fine-grained bimanual manipulation with low-cost hardware. *arXiv preprint arXiv:2304.13705*, 2023.
- Wei Zhao, Gongsheng Li, Zhefei Gong, Pengxiang Ding, Han Zhao, and Donglin Wang. Unveiling the potential of vision-language-action models with open-ended multimodal instructions. *arXiv* preprint arXiv:2505.11214, 2025.
- Ruijie Zheng, Yongyuan Liang, Shuaiyi Huang, Jianfeng Gao, Hal Daumé III, Andrey Kolobov, Furong Huang, and Jianwei Yang. Tracevla: Visual trace prompting enhances spatial-temporal awareness for generalist robotic policies. *arXiv preprint arXiv:2412.10345*, 2024.
- Zhongyi Zhou, Yichen Zhu, Minjie Zhu, Junjie Wen, Ning Liu, Zhiyuan Xu, Weibin Meng, Ran Cheng, Yaxin Peng, Chaomin Shen, et al. Chatvla: Unified multimodal understanding and robot control with vision-language-action model. *arXiv preprint arXiv:2502.14420*, 2025.
- Brianna Zitkovich, Tianhe Yu, Sichun Xu, Peng Xu, Ted Xiao, Fei Xia, Jialin Wu, Paul Wohlhart, Stefan Welker, Ayzaan Wahid, et al. Rt-2: Vision-language-action models transfer web knowledge to robotic control. In *Conference on Robot Learning*, pp. 2165–2183. PMLR, 2023.

A APPENDIX

A.1 Transformer Architecture and Late-Fusion Details

Notation. Let D be the latent dimension, h the number of heads, $d_k = D/h$. The encoder operates over a token sequence $\mathcal{X} = [x^{\text{lat}}, \, x^{\text{state}}, \, x^{\text{env}}, \, x^{\text{lang}}, \, X^{\text{img}}]$ where the first four are single 1D tokens and X^{img} is a grid of image tokens flattened to length N_{img} . We denote the encoder output by $H \in \mathbb{R}^{N \times D}$ and the decoder runs on H action query slots $Y \in \mathbb{R}^{H \times D}$ ("chunk size" in code).

Input Projections and Token Layout Each 1D modality is projected to D by a linear layer:

$$x^{\text{state}} = W_{\text{state}} s$$
, $x^{\text{env}} = W_{\text{env}} e$, $x^{\text{lang}} = l$, $x^{\text{lat}} = W_{\text{lat}} z$.

with z initialized as zeros at inference and sampled from a VAE posterior during training. Visual features come from a frozen backbone (e.g., ResNet) and are $C \times H \times W$ maps projected by a 1×1 conv W_{img} to D per spatial location, then flattened to tokens $X^{\text{img}} \in \mathbb{R}^{N_{\text{img}} \times D}$.

Positional Embeddings For 1D tokens (latent/state/env/lang), we use learned index embeddings $p_i \in \mathbb{R}^D$. For image tokens, we use 2D sinusoidal embeddings with coordinates normalized to $[0, 2\pi]$:

$$u_x(i) = 2\pi \frac{i}{W}, \quad u_y(j) = 2\pi \frac{j}{H}, \quad \omega_k = 10000^{\frac{2\lfloor k/2 \rfloor}{D/2}},$$

$$PE_x(2k) = \sin(u_x/\omega_k), PE_x(2k+1) = \cos(u_x/\omega_k), PE_y(2k) = \sin(u_y/\omega_k), PE_y(2k+1) = \cos(u_y/\omega_k),$$

and we concatenate (PE_y, PE_x) channel-wise (as in code). Decoder slots use learned positional embeddings $P^{\text{dec}} \in \mathbb{R}^{S \times D}$.

Transformer Encoder (Lightweight, Pre-Norm) We form

$$X = \operatorname{concat}([x^{\operatorname{lat}}, x^{\operatorname{state}}, x^{\operatorname{env}}, x^{\operatorname{lang}}, X^{\operatorname{img}}]) \in \mathbb{R}^{N \times D},$$

and corresponding $P^{\text{enc}} \in \mathbb{R}^{N \times D}$. Each encoder layer applies (pre-norm) multi-head self-attention (MHA) and a feed-forward network (FFN) with residuals:

$$\tilde{X} = X + \text{MHA}(\text{LN}(X) + P^{\text{enc}}, \text{LN}(X) + P^{\text{enc}}, \text{LN}(X)), \quad H = \tilde{X} + \text{FFN}(\text{LN}(\tilde{X})).$$

For a single head,

$$\operatorname{Attn}(Q,K,V) = \operatorname{softmax}\left(\frac{QK^{\top}}{\sqrt{d_{L}}}\right)V, \quad Q = (X+P^{\operatorname{enc}})W_{Q}, \ K = (X+P^{\operatorname{enc}})W_{K}, \ V = XW_{V}.$$

The encoder has $L_{\rm enc}$ layers (4 in this paper) and ends with a LayerNorm.

Transformer Decoder (Late Fusion via Cross-Attention) Decoder input is initialized as $Y^{(0)} = \mathbf{0} \in \mathbb{R}^{S \times D}$, and encoder output is denoted as \mathcal{E} . Each layer performs:

(i) Self-attn:
$$\hat{Y} = Y + \text{MHA}(\text{LN}(Y) + P^{\text{dec}}, \text{LN}(Y) + P^{\text{dec}}, \text{LN}(Y)),$$

$$\textbf{(ii) Cross-attn:} \quad \bar{Y} = \hat{Y} + \text{MHA}\big(\text{LN}(\hat{Y}) + P^{\text{dec}}, \ \text{LN}(\mathcal{E}) + P^{\text{enc}}, \ \text{LN}(\mathcal{E})\big),$$

(iii) FFN:
$$Y^{\text{out}} = \bar{Y} + \text{FFN}(\text{LN}(\bar{Y})).$$

Here cross-attention implements late fusion: queries come from decoder slots, while keys/values are the multi-modal encoder memory. We use dropout and either relu/gelu activations in the FFN, matching implementation.

Action Head After L_{dec} decoder layers and a final LayerNorm, each slot is mapped to action space with a linear head:

$$A = Y^{\text{final}} W_{\text{act}} + b_{\text{act}} \in \mathbb{R}^{H \times d_{\text{act}}}.$$

This corresponds to the per-timestep joint command (or other actuation) for a chunk of length H.

Caching and Complexity Let $C_{\rm vis}$ and $C_{\rm lang}$ be the costs of frozen vision and language encoders, and $C_{\rm dec}$ the decoder cost per step. Early fusion often recomputes both encoders each timestep: $T(C_{\rm vis}+C_{\rm lang}+C_{\rm dec})$. Our decoupled late fusion caches language (and other static 1D tokens), yielding:

$$C_{\text{ours}} = T C_{\text{vis}} + C_{\text{lang}} + T C_{\text{dec}}.$$

Theoretical per-episode speedup is

$$\mathrm{Speedup} \ = \ \frac{T(C_{\mathrm{vis}} + C_{\mathrm{lang}} + C_{\mathrm{dec}})}{T\,C_{\mathrm{vis}} + C_{\mathrm{lang}} + T\,C_{\mathrm{dec}}} \ > \ 1 \quad \mathrm{for} \ T > 1.$$

Within attention, the dominant terms are $\mathcal{O}(N^2D)$ in the encoder (small $L_{\rm enc}$) and $\mathcal{O}(HND)$ in decoder cross-attention; both are lightweight due to small SH and modest N after flattening the final backbone stage.

Variational Training Objective During Training Since our action chunking decoder predicts H actions jointly. We followed traditional action chunking process Zhao et al. (2023) to add a low-dimensional latent z per chunk turns the decoder into a conditional generative model $p_{\theta}(A_{1:H} \mid z, C)$ with context C (vision, language, state), which produces $(\mu, \log \sigma^2)$ for z, using a CLS token head:

$$q_{\phi}(z \mid \mathrm{state}, \mathrm{actions}) = \mathcal{N}\big(z; \, \mu, \, \mathrm{diag}(\sigma^2)\big), \quad \text{with } \, [\mu, \log \sigma^2] = W_{\mathrm{post}} \, h_{\mathrm{CLS}}.$$

The training loss combines action regression with a KL term:

$$\mathcal{L} = \underbrace{\frac{1}{S} \sum_{t=1}^{S} \|A_t - \hat{A}_t\|_2^2}_{\text{gatin loss}} + \beta D_{\text{KL}}(q_{\phi}(z) \parallel \mathcal{N}(0, I)).$$

This yields three benefits: (i) the KL term acts as an *information bottleneck* on z, encouraging a compact, chunk-level summary that regularizes the decoder; (ii) the stochastic z enables *multi-modal* imitation (different valid action realizations) instead of regressing to means; and (iii) a single z per chunk promotes *temporal coherence* across t=1..H.

At inference, we set z=0, so latency is identical to the non-variational path.

A.2 REAL ROBOT TASKS SETUP FOR LEROBOT

Here we provide the detailed task set up for LeRobot experiment, including language instruction and task goal. For Lerobot, we use the LeRobot SoArm-101 dual-arm system (one leader arm and one follower arm). We installed an Intel RealSense D435i RGB-D camera to provide a third-person view for the experiment. And in the experiment, we only use RGB images. We collect demonstration trajectories for 10 real-world tasks for training using LeRobot teleoperation. Each episode takes 9-18 seconds for the human operator to perform depending on the complexity of the task, which translates to 300-600 time steps given the control frequency of 30Hz. For each test trial, we randomize the initial location of the target object and repeat the experiment for 50 times to match the simulation set up. This experiment is especially challenging as LeRobot was not included the the pre-training dataset, hence it will be harder for the model to predict the action for a new embodiment. We also attached the saved video roll outs for both real-robot experiment and simulation experiment in the supplementary experiment.

Tasks included in the finetuning dataset.

- **Pick-and-place Vitamin**: *Pick up the vitamin and place it on the tray.* The trial is counted as a success only when the robot correctly places the vitamin on the tray. This task tests the model's capability for handling slippy objects. The incorrect end-effector (gripper) placement could easily cause the vitamin slipped way and miss the target.
- **Pick-and-place Banana**: *Pick up the banana and place it on the tray*. The trial is counted as a success only when the robot correctly places the banana on the tray. Unlike previous papers using plastic toy vegetables or fruits, this task tests the model's capability for handling real deformable bananas. The incorrect gripper claw angle could squeeze the banana and cause the banana damaged.

- **Pick-and-place USB**: *Pick up the USB drive and place it on the tray.* The trial is counted as a success only when the robot correctly picks up the USB drive place it on the tray. This task tests the model's capability for picking up tiny objects.
- **Pick-and-place Spoon**: *Pick up the ice-cream spoon and place it on the tray.* The trial is counted as a success only when the robot correctly picks up the ice-cream spoon place it on the tray. This task tests the model's capability for picking up irregular shaped objects.
- **Pick-and-place Tissue**: *Pick up the tissue and place it on the tray*. The trial is counted as a success only when the robot correctly picks up the tissue place it on the tray. This task tests the model's capability for picking up tiny deformable objects.
- **Pick-and-place Juice Box**: *Pick up the juice box and place it on the tray*. The trial is counted as a success only when the robot correctly picks up the juice box and place it on the tray. This task tests the model's capability for picking up regular cube shaped objects.
- Move towel: Move the towel from left to right hand side. This experiment is counted as a success when the robot succeesfully grasp the edge of the cloth and move it to the right. This task tests the model's capability for handling thin slippy objects.
- **Open Lid**: *Open the lid and put on the tray*. This experiment is counted as a success when the robot successfully grasp the deformable lib handle and place it on the tray on the right hand side. This task tests the model's capability for precepting tiny handle and pick it up.
- Close Lid: Pick up the lid from tray and close it. This experiment is counted as a success when the robot successfully grasp the deformable lib handle from the tray and put it on the jar. This task is extremely challenge as it requires precise action generation to move the lid on top of the jar and make them fit seamlessly.

Unseen tasks for generalization on out-of-distribution objects and language instruction:

- Move unseen towel: Move the towel from left to right hand side. In this experiment, we use the same language instruction as the Move Towel task, but switch the test towel into a unseen one. This task is challenging as the new object is not seen in the finetuning dataset.
- Pick-and-place hand cream: Pick up the hand cream and place it on the tray. The trial is counted as a success only when the robot correctly picks up the hand cream and place it on the tray. This task tests the model's capability for understanding both unseen language instruction and objects.

A.3 QUALITATIVE RESULTS ON SIMULATION ROLLOUTS

We present manipulation rollouts on four tasks from the LIBERO suite. Figures 7–10 qualitatively illustrate how NanoVLA recovers from common failure modes (e.g., mis-localization, slipped grasps, partial actuation) and ultimately completes long-horizon tasks. Across these examples, NanoVLA combines lightweight inference with robust error recovery.



Figure 7: **LIBERO-spatial:** *Pick up the black bowl between the plate and the ramekin and place it on the plate.* Handling failed grasp to the bowl due to wrong object location estimation.

A.4 QUALITATIVE RESULTS ON REAL ROBOT ROLLOUTS

We further evaluate NanoVLA on real-robot manipulation. Consistent with our quantitative results, the model generalizes across diverse objects, environments, and language instructions, including previously unseen instances and prompts.



Figure 8: **LIBERO-object:** *Pick up the milk and place it in the basket.* Handling slipped grasp to the milk box due to wrong object location estimation.



Figure 9: LIBERO-goal: Open the middle drawer of the cabinet. Handling stuck drawer.

Figure 11 shows continuous pick-and-place under human intervention. The system monitors a region of interest and repeatedly executes the policy; after each successful transfer to the tray, an operator relocates the object to a random position. NanoVLA re-detects the new location and completes subsequent cycles reliably, despite perturbations.

In Figure 12 we compare rollouts on a challenging vitamin pick-up task. The container is round and slippery, making it prone to slipping or tipping under contact; precise action generation is required for a stable grasp. Thanks to its continuous-action decoder, NanoVLA produces more reliable grasps than SmolVLA in these real-world trials.

Figure 13 highlights out-of-distribution (OOD) generalization. The towel task demonstrates robustness to variations in appearance under a seen instruction. The hand-cream task demonstrates generalization to both an unseen object and an unseen instruction.

Finally, Figure 14 evaluates robustness across lighting conditions. Changing illumination alters shadows and color statistics, which can confound vision-language-action policies. Nevertheless, NanoVLA consistently localizes and manipulates the target across day and night settings.

A.5 TRAINING GPU PERFORMANCE

We also evaluated the memory cost for NanoVLA and baseline, we launch the training job on 1 H20 GPU under varying batch sizes (1-32), and we measure the maximum GPU memory across training period (OpenVLA failed to run at batch 32). As shown in Figure 15a, results show that our proposed method consistently require less memory than SmolVLA due to lower trainable parameters.

Additionally, we also demonstrate the efficient training capability in Figure 15b on low computing resource device (e.g., entry level GPU RTX 3060, or edge computing device Jetson Orin Nano). Compares to existing VLAs at similar size (SmolVLA), NanoVLA achieves a significant reduction (~80% on RTX 3060, ~83% on Jetson) in training time, suggesting the effeicency of the proposed decoupling structure and caching mechanism. For reference, finetuning on LIBERO dataset usually takes 1M steps to converge, which only require 30 to 40 GPU hours on these edge devices, allowing a low-cost fine-tuning and potential on-device training and reinforcement learning.



Figure 10: **LIBERO-long:** *Put both the alphabet soup and the tomato sauce in the basket.* Handling slipped grasp to the tomato sauce can due to wrong object location estimation.



Figure 11: **Pick-place multiple vitamin.** Continuous policy execution for random object locations using NanoVLA.



Figure 12: **Pick-place vitamin task.** (Above): SmolVLA rollout. (Below): NanoVLA rollout with visual trace.



Figure 13: **OOD policy execution.** (Above): NanoVLA rollout for seen language instruction but unseen and object. (Below): NanoVLA rollout for unseen language instruction and object.



Figure 14: **Policy execution under different lighting condition.** (Above): NanoVLA rollout for policy execution during night. (Below): NanoVLA rollout for policy execution during day time.

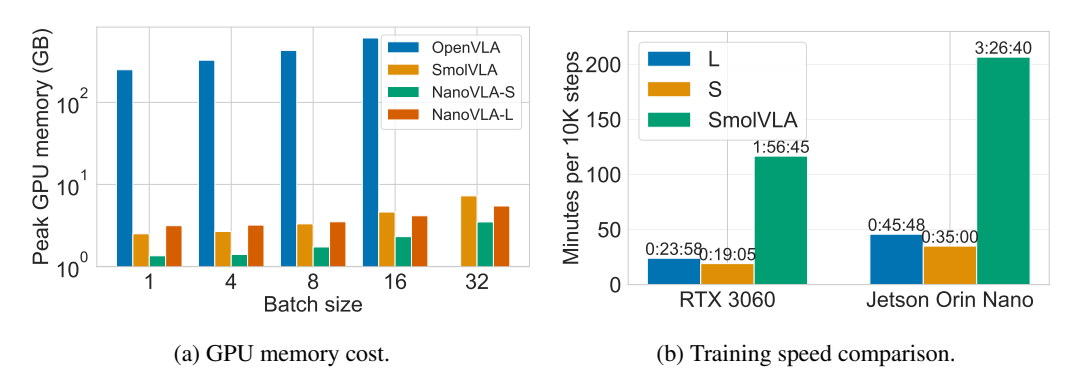


Figure 15: Computational efficiency analysis on Jetson Orin Nano.